

Article

# Microfiber-Lithium Niobate on Insulator Hybrid Waveguides for Efficient and Reconfigurable Second-Order Optical Nonlinearity on a Chip

Andrey V. Gorbach <sup>1</sup> and Wei Ding <sup>2,\*</sup>

<sup>1</sup> Department of Physics, University of Bath, Bath BA2 7AY, UK; E-Mail: A.Gorbach@bath.ac.uk

<sup>2</sup> Laboratory of Optical Physics, Institute of Physics, Chinese Academy of Sciences, Beijing 100190, China

\* Author to whom correspondence should be addressed; E-Mail: wding@iphy.ac.cn; Tel.: +86-10-8264-9427; Fax: +86-10-8264-8133.

Received: 18 July 2015 / Accepted: 2 September 2015 / Published: 9 September 2015

---

**Abstract:** We present an optical microfiber-lithium niobate on insulator (MF-LNOI) hybrid waveguide for efficient second-order nonlinear processes. The structure combines the advantages of low-loss fiber and high-nonlinearity waveguide systems. We demonstrate the possibility of phase matching between fundamental and second harmonics in a wide spectral and dimensional range, and efficient second harmonic generation over sub-millimeter propagation distances, both of which are very attractive for high-density on-chip integration.

**Keywords:** nonlinear optics; parametric processes; frequency conversion

---

## 1. Introduction

One of the most prominent characteristics of silica fibers is the exceptionally weak absorption in the infrared wavelength range. This quality makes fibers not only the key element in high-speed optical communication systems, but also an outstanding platform for nonlinear optics [1]. Second-order nonlinear effects have been observed in fibers since early 1980s [2,3]. To create an effective second order polarization, apart from strictly zero in bulk silica glass, periodic poling of fibers is commonly used [4,5]. In combination with the Quasi-Phase Matching (QPM) [6], this allows us to achieve high efficiency of second harmonic generation (SHG) [7] and parametric down-conversion [8,9] in fibers.

The latter process is a convenient tool for generation of correlated photon pairs [8–10]. It is desirable to advance efficient fiber-based photon pair sources, as they can be seamlessly connected with telecommunication systems. However, to achieve the required efficiency of second-order nonlinear processes in periodically poled fibers, one needs to use large propagation distances, typically of the order of a few dozens of centimeters [7]. This poses serious limitations to miniaturization of such nonlinear functionalities, and undermines their potential on-chip integration.

In contrast,  $\chi_2$ -crystals such as lithium niobate ( $\text{LiNbO}_3$ , LN) offer inherently strong second-order nonlinear response. As a result, efficient nonlinear effects are observed in  $\chi_2$ -crystal waveguides over propagation distances as short as few millimeters [11–14]. Recent developments in production and nano-structuring of LN thin film ( $\text{LiNbO}_3$  on Insulator, LNOI) [15,16] have led to the advancement of compact high-contrast photonic devices [17–22]. The waveguide is the fundamental structure in these devices. However, propagation losses of the LNOI waveguides are at an appreciable level of few dB/cm, and when the waveguide cross-sectional dimensions are reduced below 1  $\mu\text{m}$ , the losses rise even further to the levels of  $\sim 10$  dB/cm [17]. Periodic poling of such waveguides, required for QPM, also proves to be a challenging task [15]. Furthermore, while the period of the poling is fixed for a particular pump wavelength, this leaves no room for adjustments of individual waveguides integrated in a circuit. The conventional method of temperature control is not suitable for high-density on-chip integration because of the lack of sufficient resolution. Obviously, additional degrees of freedom for phase-matching adjustment are demanded from the viewpoint of on-chip integration.

Recently, researchers have considered the possibility to achieve second-order nonlinear response in microfibers (MFs) without periodic poling, by enhancing surface nonlinearities [23,24] or coating MF with organic molecules possessing strong second-order nonlinear response [25]. Direct phase matching was also considered for the so-called M-waveguides, which have specially engineered layered core structure [26]. The major bottleneck of such structures is in the necessity to achieve phase matching between different modes, which is only possible in a narrow interval of the pump wavelengths or fiber radius. Also, the possibility of clean chemical coating of MFs with diameters of the order of 1  $\mu\text{m}$  and below, required for phase matching, has not been demonstrated yet. However, these studies have led to an important inspiration that the QPM second-order nonlinearity, which is commonly used in weakly-guiding structures, could possibly be replaced by an inter-modal phase matching second-order nonlinearity in high-contrast waveguides. Besides, the match of the transmission windows of silica and LN (from visible to mid-infrared), and their relatively close refractive indices (at 1550 nm,  $n = 1.44$  for silica and  $n_o = 2.21$ ,  $n_e = 2.14$  for LN, in contrast to  $n = 1$  for air and  $n = 3.46$  for silicon) encourage us to explore hybrid structures composed of a microfiber and LN thin film.

In this work we introduce a MF-LNOI hybrid waveguide which features the combination of a strong second-order nonlinearity, and tunability in a wide range of wavelengths and geometrical sizes. The structure represents a free-standing X-cut LNOI waveguide [27] with the dimension of  $H \times W \times L$  attached to a side of a microfiber with the diameter  $D$ , see Figure 1. Van der Waals attraction keeps together the two parts at their relatively symmetric position [28]. When necessary, the whole structure can also be detached and reassembled at other positions along the microfiber. Note that there is no chemical treatment in the whole fabrication process, ensuring a contamination-free waveguide. By inclusion of in- and out-tapering sections in the LNOI waveguide, one can efficiently couple the

pump power into and get the SHG light out of the hybrid waveguide, avoiding insertion losses with fiber optical systems and laser damages associated with input facets of waveguides.

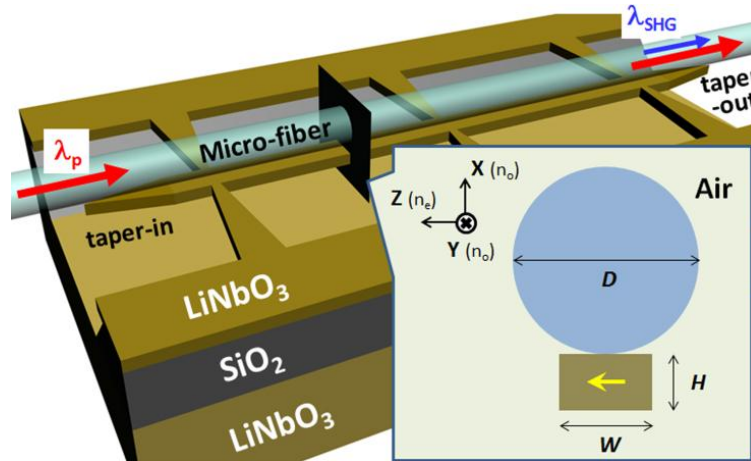


**Figure 1.** Schematic view of the microfiber-lithium niobate on insulator (MF-LNOI) hybrid waveguide. The optic axis of LN crystal is indicated by the yellow arrow.

## 2. Calculations

When the fiber diameter and the waveguide transverse dimensions are comparable to the operating wavelengths, hybridization of the fiber and the waveguide modes occurs. In this regime, a significant fraction of power in each mode enters into the LN part of the structure, thus creating a scope for potentially strong second-order nonlinear interactions, see left panels in Figure 2. Increasing the fiber diameter, the modes gradually transform into conventional fiber modes, see right panels in Figure 2.

To describe SHG process in the hybrid waveguide, we expand the total electric field as the sum of the fundamental and second harmonics,  $\vec{e} = \frac{1}{2} \frac{A_p(y)}{\sqrt{N_p}} \vec{e}_p(z, x) e^{i\beta_p y - i\omega_p t} + \frac{1}{2} \frac{A_s(y)}{\sqrt{N_s}} \vec{e}_s(z, x) e^{i\beta_s y - i\omega_s t} + c.c.$ . Here  $\omega_s = 2\omega_p$ ,  $\vec{e}_p$  and  $\vec{e}_s$  are the modal profiles,  $\beta_p$  and  $\beta_s$  are the corresponding propagation constants, normalization factors  $N_j$  ( $j = p, s$ ) are chosen such that  $|A_p|^2$  and  $|A_s|^2$  give powers carried by the fundamental and second harmonic modes in  $y$ -direction, respectively,  $N_j = \frac{1}{4} \iint_{-\infty}^{+\infty} (\vec{e}_j \times \vec{h}_j^* + \vec{e}_j^* \times \vec{h}_j) \cdot \hat{y} dz dx$ . Assuming the amplitude of the second harmonic to be much weaker than the pump, using perturbation expansion of Maxwell equations, for the slowly varying amplitude  $A_s(y)$  the following equation is obtained [23,24,29]:

$$\frac{dA_s}{dy} = i\rho_2 A_p^2 \exp(-i\Delta\beta y) \tag{1}$$

where  $\Delta\beta = \beta_s - 2\beta_p$  and the nonlinear coefficient is:

$$\rho_2 = \frac{\epsilon_0 \omega_s}{8\sqrt{N_s N_p}} \iint_{WG} (\hat{d}^{(2)} \vec{e}_p^2) \cdot \vec{e}_s^* dz dx \tag{2}$$

$\hat{d}^{(2)}$  is the reduced second-order nonlinear tensor [30], the integration is done over the LNOI waveguide area. We estimate the attenuation of the hybrid structure to be of the order of few dB/cm, mainly caused

by scatterings and absorptions of LNOI waveguide [17]. For propagation distances below 1 mm, considered in this work, we therefore can neglect attenuation in Equation (1).

We choose the optical axis of LNOI thin film to be oriented horizontally, see Figure 1. Hence modes with appreciable  $E_z$ -components inside the LN crystal experience strong nonlinearity. In Figure 2 we demonstrate the possibility of phase matching between the fundamental  $HE_{11}$ -like mode ( $HE_{11}$  mode in MF +  $TE_{00}$  mode in LNOI) at the pump wavelength  $\lambda_p = 1.5 \mu\text{m}$  and the higher order  $TE_{01}$ -like mode ( $TE_{01}$  mode in MF +  $TE_{01}$  mode in LNOI) at the second harmonic wavelength  $\lambda_s = \lambda_p/2 = 0.75 \mu\text{m}$ . Both hybrid modes in Figure 2 have dominant electric field components oriented along  $z$ -axis inside LN. In this case, the integrand in Equation (2) can be approximated as  $d_{33}e_{p,z}^2 e_{s,z}^*$  with  $d_{33} \approx 19 \text{ pm/V}$  at  $1.5 \mu\text{m}$  [31].

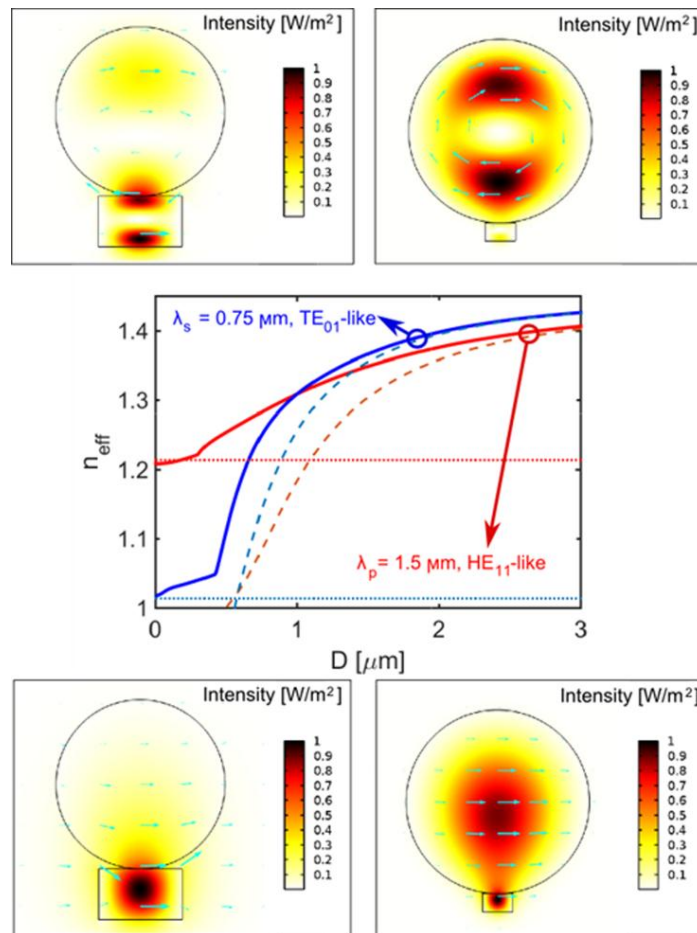


**Figure 2.**  $HE_{11}$ -like mode at  $\lambda_p = 1.5 \mu\text{m}$  and  $TE_{01}$ -like mode at  $\lambda_s = 0.75 \mu\text{m}$ : light intensity and the electric field polarization. Modal profiles are plotted for  $D = 3 \mu\text{m}$  (right panels) and  $D \approx 1 \mu\text{m}$  (corresponding to phase matching, left panels). The effective indices as functions of the fiber diameter are shown in the central panel. The waveguide dimensions are:  $H = 300 \text{ nm}$ ,  $W = 495 \text{ nm}$ . The effective indices of pure MF modes and pure LNOI waveguide modes are plotted with dashed lines and dotted lines, respectively.

In a pure MF (without LNOI), the material dispersion of silica glass (the refractive indices of silica at the two wavelengths are 1.4446 and 1.4542, respectively) can be compensated by the modal dispersion only near the cutoff of both modes:  $D \approx 0.58 \mu\text{m}$ ,  $n_{\text{eff}} \approx 1.02$ , see dashed curves in the central panel of Figure 2. In the MF-LNOI structure, the hybridization of pure MF and pure LNOI modes via the avoided

crossings shifts the phase matching to a larger MF diameter,  $D \approx 1 \mu\text{m}$ , and a considerably higher effective index,  $n_{\text{eff}} \approx 1.31$ , see solid curves in the central panel of Figure 2. While the diameter increase is important from the viewpoint of MF fabrication, the larger effective index implies a much stronger field confinement and hence more effective nonlinear interaction.

Large refractive index contrasts between silica and air, LN and air, allow guidance of light in a compact sub-micrometer scale structure, but also result in a high sensitivity of guided modes to size variations. Keeping the waveguide height  $H$  fixed, as dictated by the LNOI wafer characteristics with the variation less than 1 nm [15], there are two other geometrical parameters left to adjust propagation constants of the modes: the fiber diameter  $D$  and the waveguide width  $W$ . In Figure 3 the detuning  $\Delta\beta$  between propagation constants of the  $\text{HE}_{11}$ -like and  $\text{TE}_{01}$ -like modes is plotted as functions of  $W$ ,  $D$  and  $\lambda_p$ . The calculations were done with the help of Comsol Multiphysics, using the material dispersions of silica [1] and LN [30] available in the literature. For a fixed pump wavelength  $\lambda_p$ , the phase matching is obtained by adjustments of  $W$  and  $D$ , see Figure 3a. Likewise, one can achieve phase matching within a wide range of pump wavelength by fixing either  $D$  or  $W$ , see Figure 3b,c.

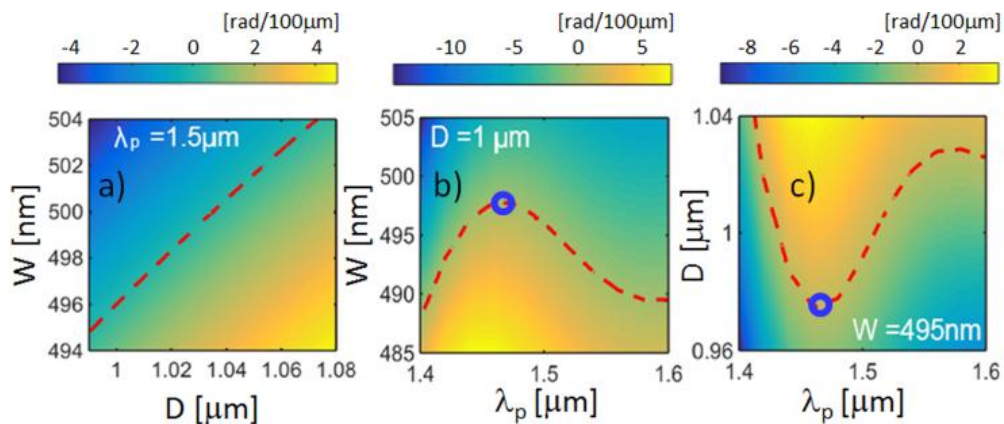


**Figure 3.** Detuning  $\Delta\beta$  between the second harmonic and pump modes as functions of pump wavelength  $\lambda_p$ , fiber diameter  $D$  and waveguide width  $W$ : (a) Fixed  $\lambda_p = 1.5 \mu\text{m}$ . (b) Fixed  $D = 1 \mu\text{m}$ . (c) Fixed  $W = 495 \text{ nm}$ . Dashed line indicates the phase matching condition  $\Delta\beta = 0$ . Broadband phase-matching is expected in the conditions marked by blue circles.

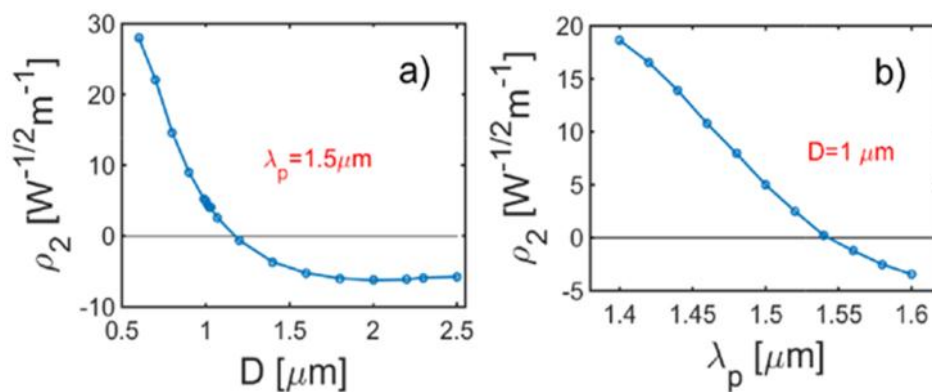


**Figure 4.** Nonlinear coefficient as function of the fiber diameter (a) Pump wavelength. (b) For the case of perfectly matched fundamental and second harmonics, cf. dashed curves in Figure 3a,b, respectively.

The direct phase matching between different modes, as opposed to QPM, removes the necessity of periodic grating structures, significantly reducing the overall waveguide size, and hence being attractive for high-density on-chip integration. However, the direct phase matching can only be achieved between the fundamental and a higher order mode. This introduces additional implications, since the electric field profiles in different modes strongly affect the resulting nonlinear coefficient in Equation (2). In particular, the overlap integral in Equation (2) between the TE<sub>00</sub> and TE<sub>01</sub> modes of an isolated LNOI waveguide (*i.e.*, free-standing and without the fiber) is strictly zero due to the different symmetries of the two modes. The introduction of the fiber, and the subsequent hybridization between the fiber and the waveguide modes, change the structure of the modes and lead to non-zero values of  $\rho_2$ . It is seen that the magnitude and sign of the resulting nonlinear coefficient are sensitive to variations in sizes and the pump wavelength, Figure 4. Crucially, the possibility to achieve phase matching in a wide range of three parameters,  $W$ ,  $D$  and  $\lambda_p$ , allows one to adjust the nonlinearity independently for the required pump wavelength or fixed fiber/waveguide dimensions.

### 3. Results and Discussion

Of all the three parameters, the waveguide width  $W$  is identified to bring the strongest variations in  $\Delta\beta$  and  $\rho_2$  both crucial for the efficiency of SHG. To investigate possible effects of random variations of the waveguide width in a realistic structure, we performed numerical integration of Equation (1) with variable coefficients  $\Delta\beta$  and  $\rho_2$  along the propagation distance. The structure was split into small sections of lengths  $L_m + \delta l_j$ , the waveguide width inside each  $j$ -th section ( $j = 1, 2, 3, \dots$ ) was fixed to  $W_m + \delta w_j$ . Here  $\delta l_j$  and  $\delta w_j$  are random perturbations. We chose the mean length of each section to be  $L_m = 10 \mu\text{m}$  with the maximal amplitude of variation  $\max(|\delta l_j|) = 5 \mu\text{m}$ . The mean waveguide width was taken as  $W_m = 442 \text{ nm}$ , which gives the phase matching at  $\lambda_p = 1.5 \mu\text{m}$  and  $D = 0.7 \mu\text{m}$ , the corresponding value of the nonlinear coefficient is  $\rho_2 = 22 W^{-1/2} m^{-1}$ , see Figure 4a. We let the variation of width to have the maximal amplitude  $\max(|\delta w_j|) = 5 \text{ nm}$ . Such level of sidewall roughness has recently been demonstrated in a dry-etched LNOI device [21]. A typical profile of the structure is shown with the light-grey curve in Figure 5. The corresponding variations of  $\Delta\beta$  and  $\rho_2$  were obtained by approximating the functions  $\Delta\beta(W)$  and  $\rho_2(W)$  with linear dependencies. The linear coefficients  $\frac{\partial(\Delta\beta)}{\partial W}(W_m) = -0.8 \cdot 10^4 \text{ rad}/(m \cdot \text{nm})$  and  $\frac{\partial\rho_2}{\partial W}(W_m) = -0.34 W^{-1/2}/(m \cdot \text{nm})$  were calculated from the numerical data in Figures 3a and 4a, respectively.

The resulting SHG conversion efficiency  $\eta = |A_s|^2/|A_p|^4$  as function of the propagation distance, averaged over 1000 realizations, is shown in Figure 5 with the solid black curve. For the ideal structure, analytical solution of Equation (1) with constant  $\Delta\beta = 0$  and  $\rho_2$  gives  $\eta_0 = \rho_2^2 y^2$  [23], see the dashed curve in Figure 5. For propagation distances below  $y \sim 200 \mu\text{m}$ , random variations do not introduce any appreciable reduction of the SHG efficiency. At the same time, while the nonlinear coefficient can be as high as  $\rho_2 \sim 22 W^{-1/2} m^{-1}$ , the efficiency of SHG in such a miniature structure is comparable to the best efficiencies achieved to date in other geometries of much larger scale, see Table 1. Note that the sub-micrometer scale cross-sectional dimension of our waveguide partly compensates the low field profile overlap.

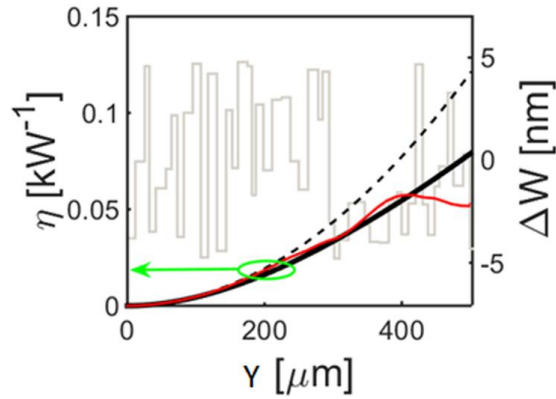


**Figure 5.** Normalized efficiency of second harmonic generation (SHG) in the structure with random variations of the waveguide width  $W$ : solid curve corresponds to  $\eta$  averaged over 1000 realizations, dashed curve indicates efficiency in the ideal structure without variations, solid red/grey curve corresponds to a particular random structure shown with the light-grey curve.

**Table 1.** Normalized SHG conversion efficiency [32],  $\eta_{\text{nor}} = \eta/L^2$ , for different geometries.

Structure	Length (mm)	$\eta_{\text{nor}}$ [%/(W cm <sup>2</sup> )]
<b>Periodically Poled Structures:</b>		
Periodically poled fiber [7]	320	$7.1 \times 10^{-5}$
Periodically poled IE KTP waveguide [11]	2.2	$2.6 \times 10^{-2}$
Periodically poled APE LN waveguide [32]	33	150
<b>Direct Phase Matching Structures:</b>		
Slot nano-fiber [24]	1.0	$2.7 \times 10^{-4}$
Organic surface coated fiber [25]	3.0	$3.4 \times 10^{-7}$
Hybrid waveguide (this work, cf. Figure 5)	0.2	4.8

As mentioned above, the weak electric field overlap between two different modes strongly affects the nonlinear coefficient. This drawback can be circumvented if we introduce alternative layers into LNOI wafers. As shown in Figure 6, when the top layer of the LNOI wafer is composed of two LN thin films with opposite  $z$ -axes, the structure parity compensates the different parities of the pump mode and the SHG mode. It is known that the fabrication of LN thin film can be done by ion-slicing or grinding processes, both having been maturely developed. Based on the new design of LNOI wafer in Figure 6, the calculated normal SHG conversion efficiency rises from 4.8 to 260 [%/(W cm<sup>2</sup>)] ( $\rho_2$  rises from 22 to 161  $W^{-1/2}m^{-1}$ ), if all the other geometric parameters are kept the same as in Figure 5. For the input power of 0.5 W, which is limited by damage threshold of LN ( $\sim 300$  MW cm<sup>-2</sup>) [30], this gives the expected power of the generated second harmonic of the order of 250  $\mu$ W. Compared to conventional Ti diffusion and (annealed) proton-exchange techniques for fabrication of waveguides in bulk LN crystal, LNOI techniques could avoid Li<sup>+</sup> deficiency and material phase change induced problems [32,33]. Moreover, LNOI and MF techniques bring high-index contrast waveguides, implying abundant dispersion engineering capabilities. In contrast, conventional LN waveguides rely on very low index contrast ( $\Delta n < 0.1$ ), and the waveguide dispersion cannot be efficiently engineered. Considering optical performance of our device under temperature variations, one should take into account temperature dependencies of the refractive indices of LN and fused silica, given by the gradients

$dn_e/dT \sim 3.5/4.1 \times 10^{-5} \text{ K}^{-1}$  [30], and  $dn/dT \sim 1.1/1.0 \times 10^{-5} \text{ K}^{-1}$  [1] at the pump/SHG wavelength, respectively. Taking into account relatively short interaction distances, we do not expect a strong variation of SHG efficiency with temperature. Detailed investigations of possible temperature related effects are beyond the scope of this work.

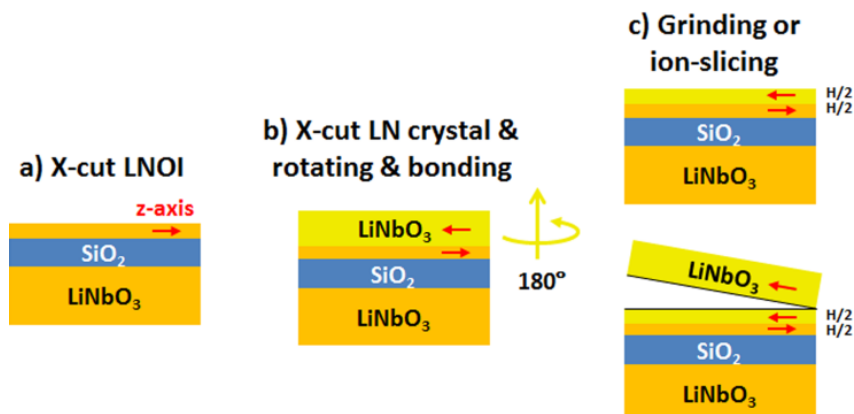


**Figure 6.** Suggested flow chart for fabrication of alternatively-layered LNOI wafer. Optic axes are indicated by red arrows. All the linear optical properties are identical with ordinary LNOI wafers.

#### 4. Conclusions

In summary, we propose a hybrid MF-LNOI waveguide suitable for efficient second-order nonlinear processes at the miniature micro-meter scale. The main advantages of this structure are: (1) low in- and out-coupling losses due to smooth integration with conventional fibers; (2) strong second-order nonlinearity over short propagation distance due to hybridization between fiber and LNOI waveguide modes; (3) two geometrical parameters to adjust independently phase matching and nonlinearity for the desired pump wavelength within a wide spectral range. The efficiency of second harmonic generation in the proposed MF-LNOI structure is demonstrated to be comparable to the best reported state-of-the-art results for other geometries, while the propagation distance is orders of magnitude shorter. We believe that the unique tunability and the overall miniature scale make the MF-LNOI structure to be an outstanding platform for potential high-density on-chip integration and development of compact and efficient SHG devices and correlated photon pair sources.

#### Acknowledgments

This work was supported by the National Natural Science Foundation of China (No. 61275044, 61575218, and 11204366), the Instrument Developing Project of the Chinese Academy of Sciences (No. YZ201346), and the State Key Laboratory of Advanced Optical Communication Systems Networks.

#### Author Contributions

Wei Ding conceived the original design of the structure and its further modification in Figure 6, and developed the manufacturing method. Andrey V. Gorbach performed phase matching analysis,

calculation of nonlinear coefficients, dynamical simulations of SHG in a random structure. Both authors contributed to scientific discussions, manuscript writing and editing.

### Conflict of Interest

The authors declare no conflict of interest.

### References

1. Agrawal, G.P. *Nonlinear Fiber Optics*, 5th ed.; Academic Press: San Diego, CA, USA, 2013.
2. Fujii, Y.; Kawasaki, B.S.; Hill, K.O.; Johnson, D.C. Sum-frequency light generation in optical fibers. *Opt. Lett.* **1980**, *5*, 48–50.
3. Ohmori, Y.; Sasaki, Y. 2-wave sum-frequency light generation in optical fibers. *IEEE J. Quantum Electron.* **1982**, *18*, 758–762.
4. Kashyap, R. Phase-matched periodic electric-field-induced second-harmonic generation in optical fibers. *J. Opt. Soc. Am. B* **1989**, *6*, 313–328.
5. Myers, R.A.; Mukherjee, N.; Brueck, S.R.J. Large second-order nonlinearity in poled fused silica. *Opt. Lett.* **1991**, *16*, 1732–1734.
6. Armstrong, J.; Bloembergen, N.; Ducuing, J.; Pershan, P. Interactions between light waves in a nonlinear dielectric. *Phys. Rev.* **1962**, *127*, 1918–1939.
7. Canagasabey, A.; Corbari, C.; Gladyshev, A.V.; Liegeois, F.; Guillemet, S.; Hernandez, Y.; Yashkov, M.V.; Kosolapov, A.; Dianov, E.M.; Ibsen, M.; *et al.* High-average-power second-harmonic generation from periodically poled silica fibers. *Opt. Lett.* **2009**, *34*, 2483–2485.
8. Bonfrate, G.; Pruneri, V.; Kazansky, P.G.; Tapster, P.; Rarity, J.G. Parametric fluorescence in periodically poled silica fibers. *Appl. Phys. Lett.* **1999**, *75*, 2356–2358.
9. Huy, K.P.; Nguyen, A.H.; Brainis, E.; Haelterman, M.; Emplit, P.; Corbari, C.; Canagasabey, A.; Ibsen, M.; Kazansky, P.D.; Deparis, O.; *et al.* Photon pair source based on parametric fluorescence in periodically poled twin-hole silica fiber. *Opt. Express* **2007**, *15*, 4419–4426.
10. Helt, L.G.; Zhu, E.Y.; Liscidini, M.; Qian, L.; Sipe, J.E. Proposal for in-fiber generation of telecom-band polarization-entangled photon pairs using a periodically poled fiber. *Opt. Lett.* **2009**, *34*, 2138–2140.
11. Mu, X.; Zotova, I.B.; Ding, Y.J.; Risk, W.P. Backward second-harmonic generation in submicron-period ion-exchanged KTiOPO<sub>4</sub> waveguide. *Opt. Commun.* **2000**, *181*, 153–159.
12. Banaszek, K.; U'Ren, A.B.; Walmsley, I.A. Generation of correlated photons in controlled spatial modes by downconversion in nonlinear waveguides. *Opt. Lett.* **2001**, *26*, 1367–1369.
13. Tanzilli, S.; de Riedmatten, H.; Tittel, W.; Baldi, P.; de Micheli, M.; Ostrowsky, D.B.; Gisin, N. Highly efficient photon-pair source using periodically poled lithium niobate waveguide. *Electron. Lett.* **2001**, *37*, 26–28.
14. Stivala, S.; Pasquazi, A.; Colace, L.; Assanto, G.; Busacca, A.C.; Cherchi, M.; Riva-Sanseverino, S.; Cino, A.C.; Parisi, A. Guided-wave frequency doubling in surface periodically poled lithium niobate: competing effects. *J. Opt. Soc. Am. B* **2007**, *24*, 1564–1570.
15. Poberaj, G.; Hu, H.; Sohler, W.; Günter, P. Lithium niobate on insulator (LNOI) for micro-photonics devices. *Laser Photonics Rev.* **2012**, *6*, 488–503.

16. Levy, M.; Osgood, R.M.; Liu, R.; Cross, L.E.; Cargill, G.S.; Kumar, A.; Bakhru, H. Fabrication of single-crystal lithium niobate films by crystal ion slicing. *Appl. Phys. Lett.* **1998**, *73*, 2293–2295.
17. Hu, H.; Ricken, R.; Sohler, W. Lithium niobate photonic wires. *Opt. Express* **2009**, *17*, 24261–24268.
18. Takigawa, R.; Higurashi, E.; Kawanishi, T.; Asano, T. Lithium niobate ridged waveguides with smooth vertical sidewalls fabricated by an ultra-precision cutting method. *Opt. Express* **2014**, *22*, 27733–27738.
19. Cai, L.; Han, H.; Zhang, S.; Hu, H.; Wang, K. Photonic crystal slab fabricated on the platform of lithium niobate-on-insulator. *Opt. Lett.* **2014**, *39*, 2094–2096.
20. Guarino, A.; Poberaj, G.; Rezzonico, D.; Degl’Innocenti, R.; Günter, P. Electro-optically tunable microring resonators in lithium niobate. *Nat. Photonics* **2007**, *1*, 407–410.
21. Wang, C.; Burek, M.J.; Lin, Z.; Atikian, H.A.; Venkataraman, V.; Huang, I.-C.; Stark, P.; Lončar, M. Integrated high quality factor lithium niobate microdisk resonators. *Opt. Express* **2014**, *22*, 30924–30933.
22. Lu, H.; Sadani, B.; Courjal, N.; Ulliac, G.; Smith, N.; Stenger, V.; Collet, M.; Baida, F.I.; Bernal, M.-P. Enhanced electro-optical lithium niobate photonic crystal wire waveguide on a smart-cut thin film. *Opt. Express* **2012**, *20*, 2974–2981.
23. Lægsgaard, J. Theory of surface second-harmonic generation in silica nanowires. *J. Opt. Soc. Am. B* **2010**, *27*, 1317–1324.
24. Luo, W.; Guo, W.; Xu, F.; Lu, Y. Efficient surface second-harmonic generation in slot micro/nano-fibers. *Opt. Express* **2013**, *21*, 11554–11561.
25. Daengngam, C.; Hofmann, M.; Liu, Z.; Wang, A.; Heflin, J.R.; Xu, Y. Demonstration of a cylindrically symmetric second-order nonlinear fiber with self-assembled organic surface layers. *Opt. Express* **2011**, *19*, 10326–10335.
26. Chowdhury, A.; McCaughan, L. Continuously Phase-Matched M-Waveguides for Second-Order Nonlinear Upconversion. *IEEE Photon. Technol. Lett.* **2000**, *12*, 486–488.
27. Diziain, S.; Geiss, R.; Zilk, M.; Schrepel, F.; Kley, E.-B.; Tünnermann, A.; Pertsch, T. Second harmonic generation in free-standing lithium niobate photonic crystal L3 cavity. *Appl. Phys. Lett.* **2013**, *103*, doi.10.1063/1.4817507.
28. Tong, L.M.; Gattass, R.R.; Ashcom, J.B.; He, S.L.; Lou, J.Y.; Shen, M.Y.; Maxwell, I.; Mazur, E. Subwavelength-diameter silica wires for low-loss optical wave guiding. *Nature* **2003**, *426*, 816–819.
29. Terhune, R.W.; Weinberger, D.A. Second-harmonic generation in fibers. *J. Opt. Soc. Am. B* **1987**, *4*, 661–674.
30. Dmitriev, V.G.; Gurzadian, G.G.; Nikogosian, D.N. *Handbook of Nonlinear Optical Crystals*, 3rd ed.; Springer-Verlag Berlin and Heidelberg GmbH & Co: Berlin, Germany, 1996.
31. Shoji, I.; Kondo, T.; Kitamoto, A.; Shirane, M.; Ito, R. Absolute scale of second-order nonlinear-optical coefficients. *J. Opt. Soc. Am. B* **1997**, *14*, 2268–2294.
32. Parameswaran, K.R.; Route, R.K.; Kurz, J.R.; Roussev, R.V.; Fejer, M.M.; Fujimura, M. Highly efficient second-harmonic generation in buried waveguides formed by annealed and reverse proton exchange in periodically poled lithium niobate. *Opt. Lett.* **2002**, *27*, 179–181.

33. Sun, J.; Xu, C.Q. Green-induced infrared absorption in annealed proton-exchanged MgO:LiNbO<sub>3</sub> waveguides. *J. Opt. Soc. Am. B* **2014**, *31*, 2779–2785.

© 2015 by the authors; licensee MDPI, Basel, Switzerland. This article is an open access article distributed under the terms and conditions of the Creative Commons Attribution license (<http://creativecommons.org/licenses/by/4.0/>).